# Photoelectron Spectroscopy of Free Polyoxoanions $Mo_6O_{19}^{2-}$ and $W_6O_{19}^{2-}$ in the Gas Phase

**Xin Yang,[†,‡] Tom Waters,[§] Xue-Bin Wang,[†,‡] Richard A. J. O'Hair,[§] Anthony G. Wedd,[§] Jun Li,*[,‡] David A. Dixon,[||] and Lai-Sheng Wang*[,†,‡]**

*Department of Physics, Washington State University, 2710 University Drive, Richland, Washington 99352, Environmental Molecular Sciences Laboratory, Pacific Northwest National Laboratory, Richland, Washington 99352, School of Chemistry, The University of Melbourne, Parkville, Victoria 3010, Australia, and Department of Chemistry, University of Alabama, Tuscaloosa, Alabama 35487*

*Received: June 4, 2004; In Final Form: August 12, 2004*

Two doubly charged polyoxoanions, $Mo_6O_{19}^{2-}$ and $W_6O_{19}^{2-}$, were observed in the gas phase using electrospray ionization. Their electronic structures were investigated using photoelectron spectroscopy and density functional calculations with relativistic effective core potentials. Each dianion was found to be highly stable despite the presence of strong intramolecular Coulomb repulsion, estimated to be about 2 eV for each system. The valence detachment features were all shown to originate from electronic excitations involving oxygen lone-pair type orbitals. Their observed energies were in excellent agreement with the theoretical vertical detachment energies calculated using time-dependent density functional theory. Despite being multiply charged, polyoxometalate oxide clusters can be studied in the gas phase, providing the opportunity for detailed benchmark theoretical studies on the electronic structures of these important transition-metal oxide systems.

## 1. Introduction

The polyoxometalate anions constitute a large class of inorganic cluster compounds and are attracting increasing attention because of their stability and diverse applications in catalysis, medicine, and materials science.[1−3] The Lindqvist anions $M_6O_{19}^{2-}$ (M = Mo, W) are of particular interest.[4] They exhibit high point group symmetry ($O_h$; Figure 1)[4−6] and have been viewed as a model for an ideal oxide surface.[7,8] Their electronic structures and stabilities have been investigated using empirical or approximate models[9−15] and most recently using density functional theory (DFT) calculations.[16−18] Aromaticity arising from (d−p)$\pi$ interactions around the $M_4O_4$ rings has been proposed to account for their high stability.[10,15,16] This (d−p)$\pi$ conjugation effect has been examined in more detail in the recent DFT study by one of us (J.L.).[16] The Lindqvist anions and their derivatives have been studied extensively in the condensed phase.[19−26] Both the $M_6O_{19}^{2-}$ anions have also been observed previously in the gas phase by electrospray ionization mass spectrometry.[27−29] However, despite the fact that most of the theoretical work has been performed on the isolated $M_6O_{19}^{2-}$ anions, the fundamental properties of these species in the gas phase have not been experimentally studied in any detail.

In this paper we report a photoelectron spectroscopy (PES) investigation of isolated $M_6O_{19}^{2-}$ (M = Mo, W) anions transported into the gas phase using electrospray ionization (ESI). The gas-phase PES data were compared to electron detachment energies calculated at the level of density functional theory (DFT) with effective core potentials being used to account for scalar relativistic effects on the metals. Excellent agreement between theory and experiment was obtained. Despite the expected strong intramolecular Coulomb repulsion due to the presence of two negative charges, both of the dianions $Mo_6O_{19}^{2-}$ and $W_6O_{19}^{2-}$ were found to be extremely stable gaseous species with respective electron binding energies of 3.4 and 3.6 eV relative to the monoanions.

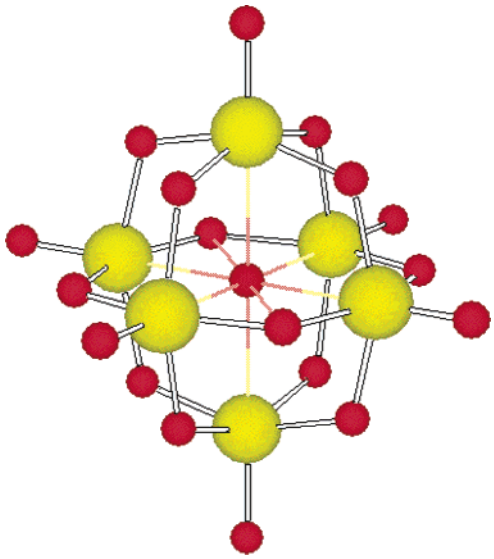

**Figure 1.** The octahedral structure of the Lindqvist polyoxoanions.

## 2. Experimental and Theoretical Methods

**2.1. Photoelectron Spectroscopy.** Experiments were performed with a magnetic-bottle type PES apparatus equipped with an ESI source. Details of the experimental apparatus have been published elsewhere.[30] Briefly, solutions of $(Bu_4N)_2[M_6O_{19}]$ (M = Mo, W) in $CH_3CN$ ($10^{-3}$ mol/L) were used for ESI in the negative ion mode with a −2.2 kV bias on the spray capillary.

* To whom correspondence should be addressed. E-mail: jun.li@pnl.gov or ls.wang@pnl.gov.
[†] Washington State University.
[‡] Pacific Northwest National Laboratory.
[§] The University of Melbourne.
[||] University of Alabama.

10.1021/jp047592i CCC: $27.50 
Published on Web 10/21/2004

The charged droplets from the electrospray nozzle were fed into a 0.5 mm diameter stainless steel desolvation capillary, which was heated to about 70 °C. The anions from the desolvation capillary were guided by a RF-only quadrupole into an ion trap, where ions were accumulated for 0.1 s before ejection into the extraction zone of a time-of-flight mass spectrometer. The $M_6O_{19}^{2-}$ dianions of interest were mass selected and decelerated before being photodetached in the interaction zone of the magnetic-bottle PES electron analyzer. Two detachment photon energies from an excimer laser were used in this study: 193 nm (6.424 eV) and 157 nm (7.866 eV). The experiments were operated at 20 Hz repetition rate with the ion beam off at alternating laser shots for background subtraction. Photoelectrons were collected at near 100% efficiency by the magnetic bottle and analyzed in a 4 m long time-of-flight tube. The photoelectron time-of-flight spectra were calibrated using the known spectra of $O^-$ and $I^-$ and converted to electron binding energy spectra by subtracting the kinetic energy spectra from the photon energies (BE = $h\nu$ − KE). The apparatus had an electron kinetic energy resolution of $\Delta KE/KE \sim 2\%$, i.e., about 10 meV for 1 eV electrons.

**2.2. Theoretical Methods.** The theoretical calculations were performed at the DFT level by using the B3LYP hybrid functional.[31−33] The inner [Ar3d$^{10}$] and [Kr4d$^{10}$4f$^{14}$] core electrons of Mo and W, respectively, were replaced by the Stuttgart small-core relativistic pseudopotentials to account for scalar relativistic effects and to reduce the computational cost for these heavy elements.[34] The standard [6s5p3d] Stuttgart pseudopotential basis sets of Mo and W were augmented by two sets of *f* and one set of *g* polarization functions.[34,35] The all-electron basis set cc-pVTZ with the [4s3p2d1f] contraction was used for O atoms throughout.[36] The geometries of $Mo_6O_{19}^{2-}$ and $Mo_6O_{19}^{2-}$ were fully optimized within $O_h$ point symmetry and vibrational frequencies were calculated via numerical differentiation methods.

Vertical electron detachment energies (VDEs) were calculated by using a combined ΔSCF-TDDFT approach previously outlined by us.[37,38] In this approach, the ground-state energies of the dianions and the monoanions were calculated from the ΔSCF energy difference at the B3LYP level, whereas the excited states of the electron-detached species were obtained from TDDFT calculations of the monoanions. The energies were calculated using the $O_h$ symmetry for the $M_6O_{19}^{2-}$ dianions, whereas those for the $M_6O_{19}^-$ anions were calculated using the $D_{4h}$ symmetry to circumvent the Jahn−Teller effects for the monoanions. In employing this ΔSCF-TDDFT approach, the selection of exchange-correlation functional is critical, particularly when anions are involved. Most commonly used local and gradient-corrected exchange-correlation potentials have the wrong asymptotic behavior due to the incorrect behavior of the exchange potential, which leads to a destabilized HOMO and thus too low an ionization potential based on the DFT version of Koopmanns' theorem. Accordingly, TDDFT calculations of excited-state energies for high-lying excited states and anionic species are known to be unreliable, as estimated ionization thresholds are too low,[39,40] and the calculated excitation energies can be underestimated by up to 1 eV.[16,41] To minimize this problem with TDDFT for the anions, we used the B3LYP(AC) self-contained asymptotic correction scheme proposed by Hirata et al. to correct the asymptotic behavior of the exchange-correlation potential.[41] In this scheme, the Casida−Salahub asymptotic correction and the Zhan−Nichols−Dixon linear correlation relation between the experimental ionization energies and the highest occupied Kohn−Sham orbital energies are used.[42,43] For all of the calculations, the extra fine integration grid was used to obtain highly accurate DFT results. All the calculations were accomplished using the NWChem 4.5 program and the Molecular Science Computing Facility (MSCF) located at the Environmental Molecular Sciences Laboratory.[44]

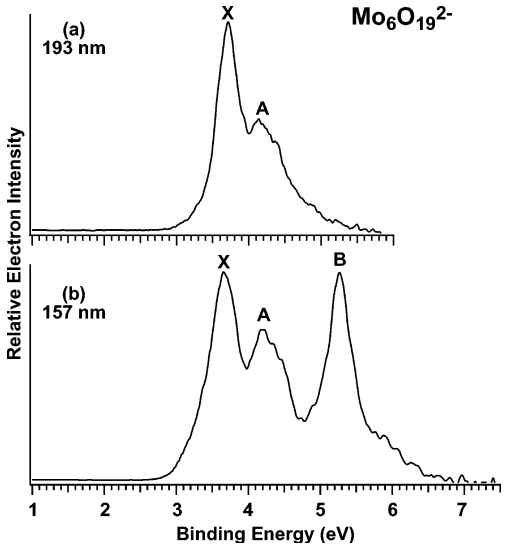


**Figure 2.** Photoelectron spectra of $Mo_6O_{19}^{2-}$ at (a) 193 nm (6.424 eV) and (b) 157 nm (7.866 eV).

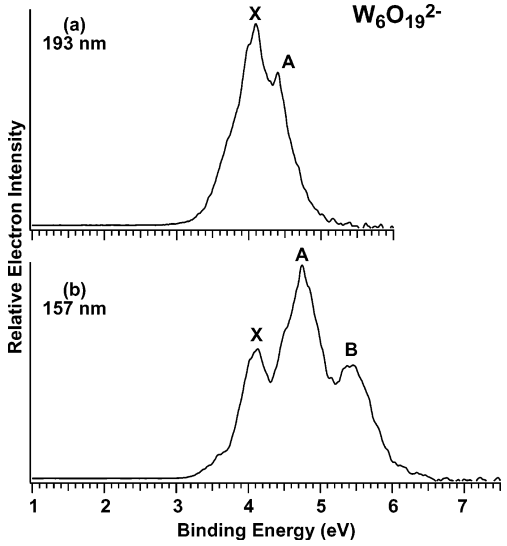


**Figure 3.** Photoelectron spectra of $W_6O_{19}^{2-}$ at (a) 193 nm (6.424 eV) and (b) 157 nm (7.866 eV).

## 3. Results

**3.1. Photoelectron Spectra.** The PES spectra of $Mo_6O_{19}^{2-}$ and $W_6O_{19}^{2-}$ are shown in Figures 2 and 3, respectively. The 157 nm spectra of both species feature three main bands (X, A, B). Each spectrum showed substantial tailing at the low binding energy side, due to the presence of hot band transitions. These are fairly large anions and appear to have significant thermal energy under our room-temperature experimental conditions. The low binding energy tailing made it more difficult to evaluate the adiabatic detachment energy (ADE). From the 193 nm data, we estimate a value of 3.4 eV for $Mo_6O_{19}^{2-}$ (Figure 2a). The electron binding energies of $W_6O_{19}^{2-}$ are higher than those of $Mo_6O_{19}^{2-}$, but the tailing in the $W_6O_{19}^{2-}$ spectra was more severe. An ADE of ∼3.6 eV was estimated for $W_6O_{19}^{2-}$.

The PES bands in the spectra shown in Figures 2 and 3 are all fairly broad. In general, if each band came from a single

electronic transition, the broad width would be an indication of large geometry changes from the dianions to the singly charged anions. However, as will be shown in the theoretical results below, the spectral widths in the current cases are most likely due to the congestion caused by multiple electronic transitions. As individual electronic transitions could not be resolved in any of the three bands, VDEs could not be obtained from these spectra.

As shown previously, the repulsive Coulomb barrier (RCB) exists universally in multiply charged anions and has a profound effect on their PES spectra.[45−47] The RCB prohibits slow electrons from being emitted and results in spectral cutoffs on the high binding energy side. This was clearly evident for the present dianions by comparison of the 193 and 157 nm spectra. Band B was absent in both spectra at 193 nm (Figures 2a and 3a) and band A in the 193 nm spectrum of $W_6O_{19}^{2-}$ was almost completely attenuated. There are likely to be more spectral transitions beyond 6 eV in the 157 nm spectra, as shown by the weak tail around 6 eV in the spectrum of $Mo_6O_{19}^{2-}$ (Figure 2b). The relatively weak intensity of band B in the 157 nm spectrum of $W_6O_{19}^{2-}$ (Figure 3b) was also likely due to the RCB. This was also the case for band A of $Mo_6O_{19}^{2-}$ in the 193 nm spectrum (Figure 2a). On the basis of these spectral intensity changes, the RCB height is estimated to be ~2 eV for each dianion. As shown previously,[48] the RCB height is equivalent to the intramolecular Coulomb repulsion present in multiply charged anions. Consequently, we can infer that each of these two dianions in the gas-phase possess Coulomb repulsion energies of about 2 eV due to the presence of the two negative charges.

**3.2. Theoretical Results.** The experimental observations for $Mo_6O_{19}^{2-}$ and $W_6O_{19}^{2-}$ in the gas phase demonstrated that these dianions are electronically and structurally stable. Calculations of the second derivatives confirmed that the free octahedral dianions possess all real frequencies and are indeed true minima. The calculated structural parameters agree well with experimental data. The optimized bond lengths are about 0.02 Å longer than those from the X-ray diffraction experiments on crystals, which is primarily due to the lack of counterions in the gas phase and is also consistent with typical deviations from experiment at the B3LYP level.

The quasirelativistic DFT energy levels of the valence occupied molecular orbitals (MOs) of both $Mo_6O_{19}^{2-}$ and $W_6O_{19}^{2-}$ are shown in Figure 4.[49] Note that all of the orbitals are bound, even though the molecules are dianions. Spin−orbit coupling effects were calculated for $W_6O_{19}^{2-}$ using the zero-order regular approach (ZORA) available in the Amsterdam density functional (ADF) program.[50,51] Spin−orbit effects induce relatively small changes for $W_6O_{19}^{2-}$ and are expected to be even less important for $Mo_6O_{19}^{2-}$. Inasmuch as spin−orbit coupling effects for $W_6O_{19}^{2-}$ are relatively small for the molecular orbital energy levels in the experimentally accessible energy region, these effects are not included in the computational simulation of the photoelectron spectra. We also calculated the first vertical detachment transitions from the valence MOs of the dianions via the ΔSCF method. The first VDEs calculated at the levels of unrestricted Hartree−Fock (UHF), Becke−Lee−Yang−Parr (BLYP), B3LYP, and B3LYP(AC) via ΔSCF energy differences are given in Table 1, and the other VDEs calculated from the ΔSCF-TDDFT approach are shown in Figure 5.

## 4. Discussion

**4.1. Comparison between the PES Spectra and TDDFT Predictions.** As shown in Figure 4, the valence occupied MOs of $Mo_6O_{19}^{2-}$ and $W_6O_{19}^{2-}$ are predicted to be similar in energy. The latter anion exhibits slightly lower orbital energies due to stronger metal−oxygen bonding. This result is in excellent agreement with the experimental observation that the tungsten oxide cluster possesses higher binding energies than its molybdenum analogue. Two groups of MOs near the HOMO are well separated from the more deeply lying MOs. The first group consists of the triply degenerate HOMO $4t_{1g}$ and HOMO-1 $11t_{1u}$, whereas the second group ($5t_{2g}$, $10t_{1u}$, and $5t_{2u}$), again all triply degenerate, lies about 0.8 eV below. The next group of MOs ($7e_g$, $1e_u$, $9t_{1u}$, and $3t_{1g}$) is about 1.6 eV below the HOMO. These energy-level patterns of the valence MOs agree qualitatively with the observed PES spectra shown in Figures 2 and 3. Bands X, A, and B can be assigned to electron detachment transitions from the MO groups ($4t_{1g}$, $11t_{1u}$), ($5t_{2g}$, $10t_{1u}$, $5t_{2u}$), and ($7e_g$, $1e_u$, $9t_{1u}$, $3t_{1g}$), respectively. The more deeply lying MOs from $7a_{1g}$ down to $7t_{1u}$ are likely to be within the 157 nm photon energy range, but as discussed above, observation of detachments from these MOs was prohibited by the RCB.

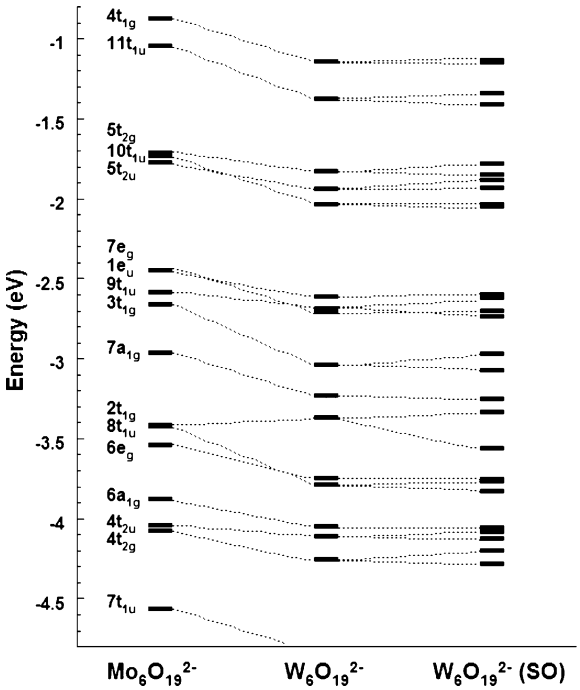


**Figure 4.** Energy levels of the occupied valence molecular orbitals of $Mo_6O_{19}^{2-}$ and $W_6O_{19}^{2-}$. For $W_6O_{19}^{2-}$ the spin−orbit splittings of the molecular orbitals are also shown (see ref 49).

**TABLE 1: Calculated First Vertical Detachment Energies for $Mo_6O_{19}^{2-}$ and $W_6O_{19}^{2-}$ Dianions at Different Levels of Theory[a]**

| | $Mo_6O_{19}^{2-}$ | $W_6O_{19}^{2-}$ |
|---|---|---|
| UHF | 4.56 | 5.37 |
| BLYP | 2.59 | 2.87 |
| B3LYP | 3.33 | 3.69 |
| B3LYP(AC) | 3.37 | 3.72 |

[a] All the energies are in eV. The $O_h$ and $D_{4h}$ symmetries were used for the dianions and monoanions, respectively.

The high symmetry of the $M_6O_{19}^{2-}$ clusters led to the high degeneracies of their valence MOs. Consequently, the first-order Jahn−Teller effect is expected to influence electron detachment from the doubly charged anions, leading to structural distortions and splittings in the final ground and excited states of the singly charged anions. However, as the HOMOs of the $M_6O_{19}^{2-}$ anions are nonbonding lone pair orbitals (see below), the Jahn−Teller structural distortion is expected to be small. As a result, the

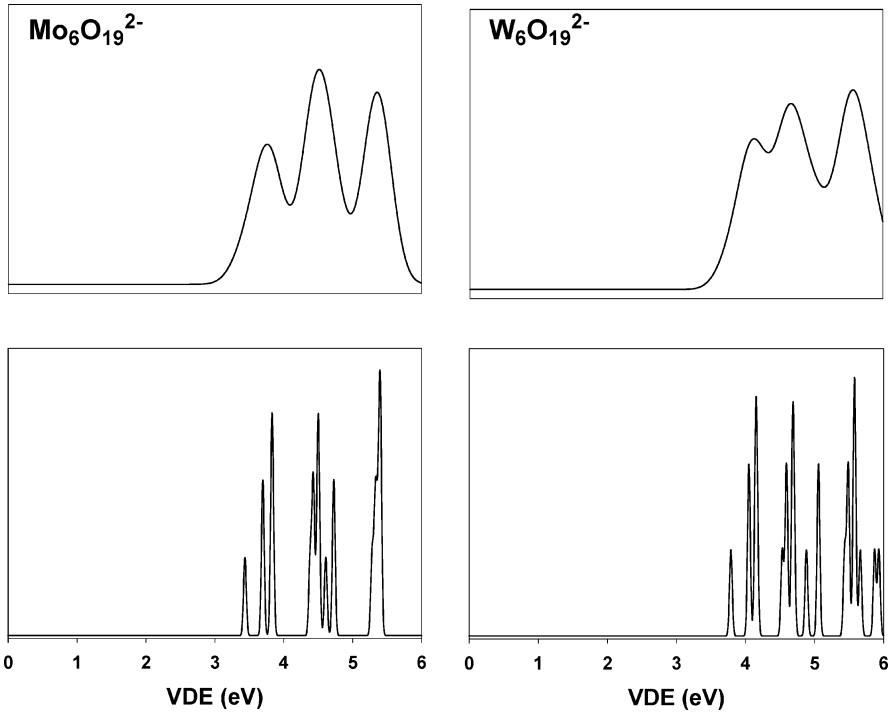


**Figure 5.** Theoretically simulated photoelectron spectra for $Mo_6O_{19}^{2-}$ and $W_6O_{19}^{2-}$. The upper and lower curves are the results when each vertical transition was convoluted with a Guassian of widths 0.2 and 0.02 eV, respectively.

VDEs and the ADEs of these dianions should be very close to each other. Indeed, as listed in Table 1, the calculated VDEs for band X are 3.33 and 3.69 eV at the B3LYP level, which are close to the experimentally estimated ADEs of 3.4 and 3.6 eV. Although the structural distortion is small, the Jahn−Teller effect does give rise to splittings in the calculated VDEs. Our state-to-state calculations via the ΔSCF-TDDFT approach clearly showed the splittings in the final states of the electron-detached species (Figure 5), with the calculated splittings of the lowest energy bands in Figure 5 (corresponding to bands X) being 0.26 eV for both metal clusters. The calculated VDEs using the B3LYP and B3LYP(AC) methods for the bands X are similar, whereas those using the UHF and BLYP methods appear to be overestimated and underestimated, respectively (See Table 1). It is important to note that the calculated state-to-state VDE spectra are in excellent agreement with the observed PES spectra. This indicates that the self-contained asymptotic correction scheme works well for calculating the anions and their excited states, as has been shown for other anionic systems.[52]

**4.2. Nature of the Valence MOs of $M_6O_{19}^{2-}$.** MO analyses for the Lindqvist metal oxide clusters have been presented in recent publications.[16−18] The LUMO ($2e_u$) is an antibonding orbital involving metal and bridging-oxygen atoms. Since the photoelectron experiments involve only the occupied MOs, Figure 6 depicts the three-dimensional contours of the occupied frontier MOs of $Mo_6O_{19}^{2-}$. The HOMO $4t_{1g}$ is mainly formed from the lone pairs of the bridging oxygen atoms. The HOMO-1 has a large contribution from the central oxygen atom, smaller contributions from the bridging oxygen atoms, and even smaller ones from the terminal $\mu$-oxo groups. The HOMO-2 and HOMO-4 have significant contributions from both the bridging and terminal oxygen atoms. The HOMO-3 is also localized on the bridging oxygen atoms. In fact, among the three groups of valence MOs accessed in the photodetachment in the current study, all but the HOMO-6 ($1e_u$) are formed from the oxygen lone pairs of the bridging, terminal, and central oxygen atoms. The $1e_u$ MO is a bonding orbital from the metal and bridging oxygen atoms and is one of the MOs responsible for the bonding in the $M_4O_4$ rings in $M_6O_{19}^{2-}$.

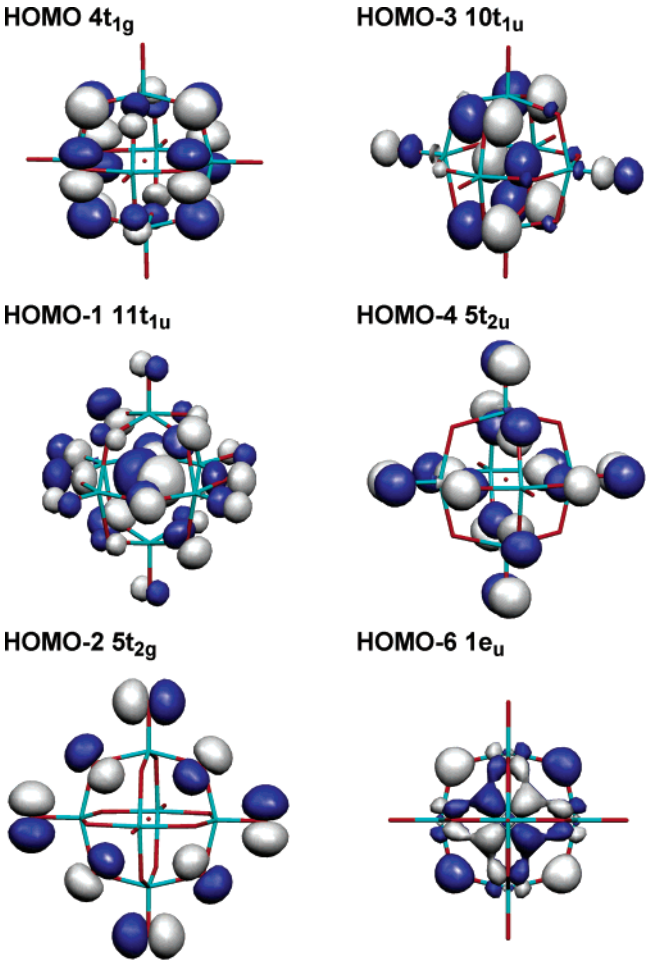


**Figure 6.** Three-dimensional contours of the occupied frontier molecular orbitals of $Mo_6O_{19}^{2-}$.

## 5. Conclusions

We report a photoelectron spectroscopic study of two polyoxoanions, $Mo_6O_{19}^{2-}$ and $W_6O_{19}^{2-}$, in the gas phase as isolated species. Both anions are highly stable in the gas phase, despite the strong intracluster Coulomb repulsion, determined experimentally to be about 2 eV. The photoelectron spectra revealed the valence electronic structures of these oxide clusters and were compared to time dependent density functional theory calculations with an asymptotically corrected functional. The vertical electron detachment energies calculated from the TDDFT method with the self-contained asymptotic correction scheme were in excellent agreement with the photoelectron spectra. This scheme was shown to be suitable to treat large anionic metal oxide cluster systems. Despite being multiply charged, polyoxometalate oxide clusters can be studied in the gas phase, providing the opportunity for detailed benchmark theoretical studies on the electronic structures of these important transition-metal oxide systems.

**Acknowledgment.** We are grateful to Dr. So Hirata (Pacific Northwest National Laboratory) for helpful discussions. All calculations were performed using supercomputers at the Molecular Sciences Computing Facility of the EMSL. This work was supported by the Chemical Sciences, Geosciences and Biosciences Division, Office of Basic Energy Sciences, U.S. Department of Energy under grant No. DE-FG02-03ER15481 and was performed at the W. R. Wiley Environmental Molecular Sciences Laboratory, a national scientific user facility sponsored by the DOE's Office of Biological and Environmental Research and located at Pacific Northwest National Laboratory, operated for the DOE by Battelle.

## References and Notes

(1) Pope, M. T. *Heteropoly and Isopoly Oxometalates*; Springer-Verlag: Berlin, 1983.
(2) Pope, M. T.; Müller, A. *Angew. Chem., Int. Ed. Engl.* **1991**, *30*, 34.
(3) *Chem. Rev.* **1998**, *98*, 1−390. A special issue on polyoxometalates edited by Hill, C. L.
(4) Lindqvist, I. *Arkiv Kemi* **1950**, *5*, 247.
(5) Allcock, H. R.; Bissell, E. C.; Shawl, E. T. *Inorg. Chem.* **1973**, *12*, 2963.
(6) Fuchs, J.; Feiwald, W.; Hartl, H. *Acta Crystallogr. B* **1978**, *34*, 1764.
(7) Day, V. W.; Klemperer, W. G. *Science* **1985**, *228*, 533.
(8) Klemperer, W. G.; Wall, C. G. *Chem. Rev.* **1998**, *98*, 297.
(9) Nomiya, K.; Miwa, M. *Polyhedron* **1984**, *3*, 341.
(10) King, R. B. *Inorg. Chem.* **1991**, *30*, 4437.
(11) Masure, D.; Chaquin, P.; Louis, C.; Che, M.; Fournier, M. *J. Catalysis* **1989**, *119*, 415.
(12) Calhorda, M. J. *J. Organomet. Chem.* **1994**, *475*, 149−155.
(13) Rohmer, M. M.; Bénard, M.; Blaudeau, J. P.; Maestre, J. M.; Poblet, J. M. *Coord. Chem. Rev.* **1998**, *178*−*180*, 1019.
(14) Dolbecq, A.; Guirauden, A.; Fourmigué, M.; Boubeckeur, K.; Batail, P.; Rohmer, M. M.; Bénard, M.; Coulon, C.; Sallé, M.; Blanchard, P. *J. Chem. Soc., Dalton Trans.* **1999**, 1241.
(15) Cai, T.; Chen, Z. D.; Wang, X. Z.; Li, L. M.; Lu, J. X. *Prog. Nat. Sci.* **1997**, *7*, 554.
(16) Li, J. *J. Cluster Sci.* **2002**, *13*, 137.
(17) Bridgeman, A. J.; Cavigliasso, G. *Inorg. Chem.* **2002**, *41*, 1761.
(18) Bridgeman, A. J.; Cavigliasso, G. *J. Phys. Chem.* A **2003**, *107*, 4568.
(19) Sanchez, C.; Livage, J.; Launay, J. P.; Fournier, M.; Jeanin, Y. *J. Am. Chem. Soc.* **1982**, *104*, 3194.
(20) Du, Y.; Rheingold, A. L.; Maatta, E. A. *J. Am. Chem. Soc.* **1992**, *114*, 345.
(21) Stark, J. L.; Young, Jr., V. G.; Maatta, E. A. *Angew. Chem., Int. Ed. Engl.* **1995**, *34*, 2547.
(22) Xu, X. X.; You, X. Z.; Huang, X. Y. *Polyhedron* **1995**, *14*, 1815.
(23) Hill, C. L.; Prosser-McCartha, C. M. *Coord. Chem. Rev.* **1995**, *143*, 407.
(24) Gouzerh, P.; Proust, A. *Chem. Rev.* **1998**, *98*, 77.
(25) Bustos, C.; Hasenknopf, B.; Thouvenot, R.; Vaissermann, J.; Proust, A.; Gouzerh, P. *Eur. J. Inorg. Chem.* **2003**, 2757.
(26) Poblet, J. M.; Lopez, X.; Bo, C. *Chem. Soc. Rev.* **2003**, *32*, 297.
(27) Lau, T.-C.; Wang, J.; Guevremont, R.; Siu, K. W. M. *Chem. Commun.* **1995**, 877.
(28) Deery, M. J.; Howarth, O. W.; Jennings, K. R. *J. Chem. Soc., Dalton Trans.* **1997**, 4783.
(29) Walanda, D. K.; Burns, R. C.; Lawrance, G. A.; von Nagy-Felsobuki, E. I. *J. Chem. Soc., Dalton Trans.* **1999**, 311.
(30) Wang, L. S., Ding, C. F.; Wang, X. B.; Barlow, S. E. *Rev. Sci. Instrum.* **1999**, *70*, 1957.
(31) Becke, A. D. *J. Chem. Phys.* **1993**, *98*, 1372/5648.
(32) Lee, C.; Yang, G.; Parr, R. G. *Phys. Rev. B* **1988**, *37*, 785.
(33) Stephens, P. J.; Devlin, F. J.; Chabalowski, C. F.; Frisch, M. J. *J. Phys. Chem.* **1994**, *98*, 11623.
(34) Andrae, D.; Haeussermann, U.; Dolg, M.; Stoll, H.; Preuss, H. *Theor. Chim. Acta* **1990**, *77*, 123.
(35) Martin, J. M. L.; Sundermann, A. *J. Chem. Phys.* **2001**, *114*, 3408.
(36) Dunning, T. H., Jr. *J. Chem. Phys.* **1989**, *90*, 1007.
(37) Li, J.; Li, X.; Zhai, H. J.; Wang, L. S. *Science* **2003**, *299*, 864.
(38) Li, X.; Kiran, B.; Li, J.; Zhai, H. J.; Wang, L. S. *Angew. Chem., Int. Ed.* **2002**, *41*, 4786.
(39) Casida, M. E.; Jamorski, C.; Casida, K. C.; Salahub, D. R. *J. Chem. Phys.* **1998**, *108*, 4439.
(40) Tozer, D. J.; Handy, N. C. *J. Chem. Phys.* **1998**, *109*, 10180.
(41) Hirata, S.; Zhan, C.-G.; Apra, E.; Windus, T. L.; Dixon, D. A. *J. Phys. Chem. A* **2003**, *107*, 10154.
(42) Casida, M. E.; Salahub, D. R. *J. Chem. Phys.* **2000**, *113*, 8918.
(43) Zhan, C.-G.; Nichols, J. A.; Dixon, D. A. *J. Phys. Chem. A* **2003**, *107*, 4184.
(44) Straatsma, T. P.; Apra, E.; Windus, T. L.; Dupuis, M.; Bylaska, E. J.; de Jong, W.; Hirata, S.; Smith, D. M. A.; Hackler, M. T.; Pollack, L.; Harrison, R. J.; Nieplocha, J.; Tipparaju, V.; Krishnan, M.; Brown, E.; Cisneros, G.; Fann, G. I.; Fruchtl, H.; Garza, J.; Hirao, K.; Kendall, R.; Nichols, J. A.; Tsemekhman, K.; Valiev, M.; Wolinski, K.; Anchell, J.; Bernholdt, D.; Borowski, P.; Clark, T.; Clerc, D.; Dachsel, H.; Deegan, M.; Dyall, K.; Elwood, D.; Glendening, E.; Gutowski, M.; Hess, A.; Jaffe, J.; Johnson, B.; Ju, J.; Kobayashi, R.; Kutteh, R.; Lin, Z.; Littlefield, R.; Long, X.; Meng, B.; Nakajima, T.; Niu, S.; Rosing, M.; Sandrone, G.; Stave, M.; Taylor, H.; Thomas, G.; van Lenthe, J.; Wong, A.; Zhang, Z. *NWChem, A Computational Chemistry Package for Parallel Computers*, Version 4.5; Pacific Northwest National Laboratory: Richland, WA, 2003.
(45) Wang, X. B.; Ding, C. F.; Wang, L. S. *Phys. Rev. Lett.* **1998**, *81*, 3351.
(46) Wang, X. B.; Wang, L. S. *Nature* **1999**, *400*, 245.
(47) Wang, L. S.; Wang, X. B. *J. Phys. Chem. A* **2000**, *104*, 1978.
(48) Wang, L. S.; Ding, C. F.; Wang, X. B.; Nicholas, J. B. *Phys. Rev. Lett.* **1998**, *81*, 2667.
(49) Since the B3LYP energy levels for these ions are very similar to the PW91 energy levels calculated via the ADF program, we plotted the energy levels from the ADF calculations, which can also provide the spin−orbit splittings of the scalar relativistic levels. For details of these calculations, see ref 16.
(50) ADF 2003.01, SCM, Theoretical Chemistry, Vrije Universiteit, Amsterdam, The Netherlands (http://www.scm.com).
(51) van Lenthe, E.; Baerends, E. J.; Snijders, J. G. *J. Chem. Phys.* **1993**, *99*, 4597.
(52) Zhai, H. J.; Li, J.; Wang, L. S. *J. Chem. Phys.* **2004**, *121*, Oct. 22.